RESEARCH ARTICLE

ZHU Dunshen, SHOU Xingxian, LIU Yixin, CHEN Erqiang, Stephen Zhengdi Cheng

AFM-tip-induced crystallization of poly(ethylene oxide) melt droplets

Abstract The AFM-tip-induced crystallization of poly(ethylene oxide) (PEO) melt droplets was studied. The melt droplets with a height of 50–100 nm and a lateral size of 2–3 μm were obtained by melting the PEO ultra-thin films on a mica surface. For the PEO samples with average molecular weights (M_n) ranging from 1.0×10^3 g/mol to 1.0×10^4 g/mol, the lateral perturbation from the AFM tip in the hard-tapping or nanoscratch modes could not induce the growth of the flat-on lamellae. In contrast, under AFM nanoindentation mode, the tip-induced crystallization occurred when a sufficiently high vertical tip force was applied to the melt droplets of PEO with $M_n \geqslant 1.0 \times 10^4$ g/mol. Moreover, the experimental results indicated that the AFM-tip-induced crystallization of PEO in the nanoindentation process had molecular weight dependence.

Keywords atomic force microscopy, poly(ethylene oxide), tip-induced crystallization, nanoindentation

1 Introduction

Atomic force microscopy (AFM), as an important tool, has been widely used in the polymer crystallization field. Usually, in order to truly reflect the crystal morphology and crystallization process, the influence from the AFM tip during scan should be minimized. On the other hand, AFM-tip-induced nucleation and the crystal growth of polymers have been also studied. It is expected that the considerable lateral force in the

ZHU Dunshen, SHOU Xingxian, LIU Yixin, CHEN Erqiang (✉), Stephen Zhengdi Cheng
Department of Polymer and Engineering, Key Laboratory of Polymer Chemistry and Physics of Ministry of Education, College of Chemistry and Molecular Engineering, Peking University, Beijing 100871, China
E-mail: eqchen@pku.edu.cn

Stephen Zhengdi Cheng
Maurice Morton Institute and Department of Polymer Science, University of Akron, Akron, Ohio 44325-3909, USA

AFM contact mode may increase the probability of tip-induced nucleation. Pearce and Vancso [1,2] reported that the AFM tip could not induce poly(ethylene oxide) (PEO) crystallization. However, for poly(ε-caprolactone) (PCL), Beekmans et al. [3] observed the AFM-tip-induced nucleation of the PCL chains, which further resulted in the growth of edge-on crystals normal to the scan direction. The above two different results arise from their difference in strength of lateral forces applied in the AFM experiments. In the AFM tapping mode, the tip has weaker interaction with the sample due to the small tip-to-sample force. Li and coworkers [4,5] found there was no evidence of tip-induced crystallization in the amorphous region around the crystal at a high undercooling ($\Delta T = {\sim}60°C$), using tapping mode. A similar observation was reported by Godovsky and Magonov [7] in polyethylene crystallization. However, according to Magonov et al., the AFM tip could penetrate the sample surface to touch the crystalline core when the applied force was increased from light-tapping to hard-tapping. Therefore, the AFM tip in tapping mode may also affect the polymer crystallization kinetics greatly and even induce polymer chains to pack together to form a nuclei in the melt. Here we report our investigation on AFM-tip-induced crystallization by lateral and vertical interactions between the AFM tip and the PEO melt droplets on a mica surface. The PEO melt droplets possessed a height ranging from 50 to 100 nm and a lateral size of 2–3 μm. The lateral perturbation was realized in hard-tapping mode or nanoscratch mode, and the vertical perturbation was done in the nanoindentation mode. The results obtained may shed some light on the control of polymer crystallization using *in situ* AFM technique.

2 Experimental

In this paper, a series of low molecular weight (LMW) PEO fractions with –OH groups on both chain ends were purchased from Polymer Source or Polymer Laboratory, of which the M_n ranged from 1.0×10^3 to 1.0×10^4 g/mol, and the polydispersities are less than 1.1. A relatively high molecular weight PEO sample with M_n of 1.0×10^5 g/mol was purchased from Aldrich. The ultra-thin films of the PEO samples on the

freshly cleaved mica surfaces were prepared by the static solution casting method. Typically, a drop of the PEO/CHCl$_3$ or PEO/CH$_2$Cl$_2$ solutions with a concentration of 0.5 mg/mL was pipetted onto the substrate; the excess solution was blotted by filter paper. The samples were then dried under ambient conditions and later in vacuum for more than 24 h. An AFM (DI Nanoscope IIIa) coupled with a hot stage was utilized to examine the morphology, melting, and crystallization behavior of the samples. NONCONTACT silicon cantilevers (model: NSC11/51, spring constant: 1.5–3.0 N/m) from MicoMasch were used to conduct the nanoindentation experiments.

3 Results and discussion

The as-cast ultrathin PEO films on the mica surface were finger-like flat-on monolayer crystals (Fig. 1(a)) with a thickness of 5–7 nm. After the films were melted, a number of PEO melt droplets on the mica surfaces could be observed by tapping mode AFM (Fig. 1(b)). The PEO melt on the hydrophilic mica surface is "pseudo-dewetting" [8–10], wherein the PEO molecules directly adsorbed on the substrate form a continuous thin wetting layer, and the rest of the material, partially wetting on the adsorbed layer, forms droplets. It is believed that high surface energy substrates such as the mica surface can strongly interact with the adsorbed PEO chains, leading to an oriented adsorption of the PEO wetting layer with a lower surface energy. The difference of chain conformation between the PEO in and out of the adsorbed layer causes the "autophobic" behavior [8], leading to the formation of the melt droplets. Depending on experimental conditions, we found that the melt droplets could have the lateral size from several hundreds of nanometers to tens of micrometers and the height of 30–200 nm. As the tapping mode AFM generally gives the topography information of the sample surface, only the melt droplets can be seen under AFM. We performed X-ray reflection (XRR) experiments to detect the adsorbed wetting layer, of which the thickness was measured to be ~4.5 nm. The "pseudo-dewetting" melt of

PEO usually crystallized into flat-on monolayer lamellae with the PEO chain direction perpendicular to the mica surface [9–12].

In the AFM tapping mode, r_{sp} is the ratio of the set-point amplitude to the driving amplitude. The effective tip-to-sample force increases with decreasing r_{sp}. When r_{sp} is larger than 0.5 for light- and moderate-tapping, i.e., the tip-to-sample force is low, only the outer-most layer morphology is detected. When r_{sp} is decreased to 0.3 or below for hard-tapping, the tip can penetrate into melt droplets. Consequently, if a crystal is embedded in a droplet, the crystal can be distinguished from the melt by the hard-tapping AFM. For the samples studied, the isothermal crystallization of the completely melted samples on the mica surface was found to be very difficult at a crystallization temperature (T_c) above 40°C. Under this condition, it is intriguing to see whether the AFM tip can induce the PEO crystallization. We used the tip to perturb the melt droplets repeatedly during scan at a T_c above 40°C in the hard-tapping mode. To further increase the lateral force, the scratch command in AFM force mode was also applied. With a controlled force to the probe, the tip scratched the melt droplets in the plane (x-y plane) parallel to the substrate. However, in both of the AFM modes, no crystallization of the LMW PEO samples ($M_n \leqslant 1.0 \times 10^4$ g/mol) was induced. Recall that the PEO ultrathin film crystallization results in the flat-on lamellae with a vertical chain direction (z direction). We consider that the AFM tip perturbation in the x-y plane cannot effectively assist PEO chains to crystallize on the mica surface.

Growing a flat-on PEO lamella requires the chains to be aligned vertically to form the nucleus first. Therefore, we consider that using the nanoindentation function of AFM, which can provide a perturbation in the z direction, may increase the possibility to induce crystallization of the melt droplets. As schematically depicted in Fig. 2, the interaction between tip and melt droplets along the z direction exists when the tip is either indented into or pulled out of the melt droplet. Especially, during pulling out, the PEO chains adhering to the tip are subjected to a tensile stress. In this case, the chains may be oriented to form the nucleus.
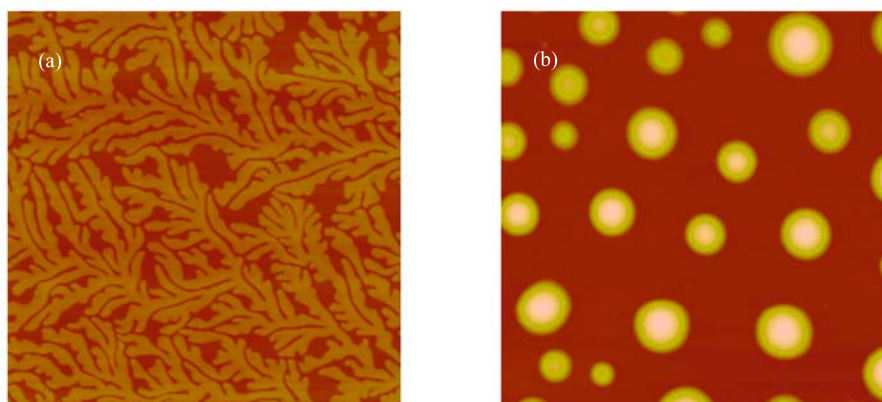

Fig. 1 Typical AFM height images of (a) an as-cast PEO ultra-thin film and (b) a pseudo-dewetted melt on the mica surfaces
The images were obtained from the PEO with M_n of 1.0×10^4 g/mol; The thickness of the dendritic monolayer in (a) is 6–7 nm; The height of the melt droplets in (b) ranges from 50 nm to 130 nm; The sizes of the images are (a) 10 μm × 10 μm and (b) 20 μm × 20 μm.
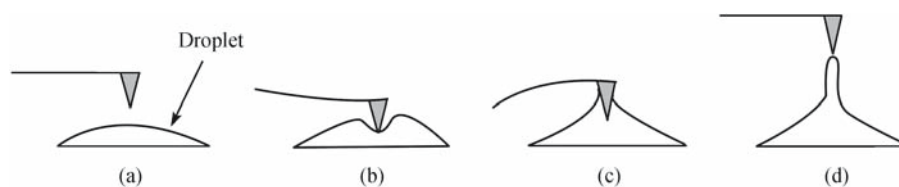
Fig. 2 Schematic illustration of the AFM-tip indentation onto the melt droplet

The detailed procedure of nanoindentation is as follows: (1) choose a region containing the flat-on crystals at room temperature with a size of typically $20\,\mu m \times 20\,\mu m$; (2) increase the AFM hot stage temperature to 75°C, and the sample temperature is then kept at 75°C for nearly 1 h to ensure complete melting; (3) decrease the temperature to a selected T_c (>40°C) wherein no primary nucleation will occur in the supercooled melt; (4) since the tip may be contaminated during scan if melt droplet is too high, select a melt droplet with a suitable size (diameter: 2–$3\,\mu m$, height: 50–100 nm.) by using the offset command in the tapping mode to move the selected droplet to the center of the image (the default position of nanoindentation), and then scan continuously until the position offset between the latest two images is less than $0.5\,\mu m$; (5) switch to the nanoindentation mode, adjusting the trig threshold to 0.2 V (the tip-to-sample force and the penetrating depth of the tip increases by increasing this value), and go back to the tapping mode to check the morphology change of the melt droplet after doing nanoindentation. If the droplet morphology remains, we increase the force with a step of 0.05–0.1 V and repeat the above operation. Note that the trig threshold cannot exceed 2.5 V. If the melt droplet cannot crystallize at T_c when the trig threshold approaches its maximum value, we decrease T_c and then repeat the procedure of (5).

Figures 3(a) and 3(b) show two AFM height images before and after nanoindentation of a PEO ($M_n = 1.0 \times 10^4$ g/mol) melt droplet at $T_c = 55$°C, respectively. The melt droplet located at the center of Fig. 3(a) with the height of 60 nm and lateral size of $2.7\,\mu m$ is suitable for our nanoindentation experiment. As shown in Fig. 3(b), a flat-on crystal of the PEO is observed in tapping mode after the nanoindentation trig threshold is increased to 0.6 V. Moreover, a cone-like nucleus with a height of 52 nm can be seen at the center of the crystal (i.e., nanoindentation position). This result implies that when the tip was pulled out of the melt droplet, the PEO chains sticking to the tip were stretched and thus turned to form the nucleus. The thickness near the edge of the flat-on crystal is 23–25 nm, corresponding to a non-integral folded-chain (NIF) crystal of the PEO sample. The formation of the NIF crystal might be due to the fast crystallization of the melt droplet induced by the nucleus. The lateral size of the PEO crystal increases with time during subsequent isothermal crystallization. The newly formed lamella may adopt the integral-folded chain [IF(n), n is the fold number] conformation that maximizes the crystal growth rate at a selected T_c. Figure 3(c) is an AFM height image obtained 21.5 min later after nanoindentation, wherein the NIF crystal is found to be surrounded by an IF(3) crystal with a thickness of 15 nm. The overall shape of the flat-on crystal looks hexagonal, with only a pair of (100) planes and other planes more or less rounded. Moreover, compared with that in Fig. 3(b), the small melt droplets around the crystal decrease in size or even disappear in Fig. 3(c). This indicates that the molten PEO molecules in the melt droplets nearby were consumed gradually by the crystal growth.

The same nanoindentation experiments were carried out for the PEO fractions with M_n less than 1.0×10^4 g/mol

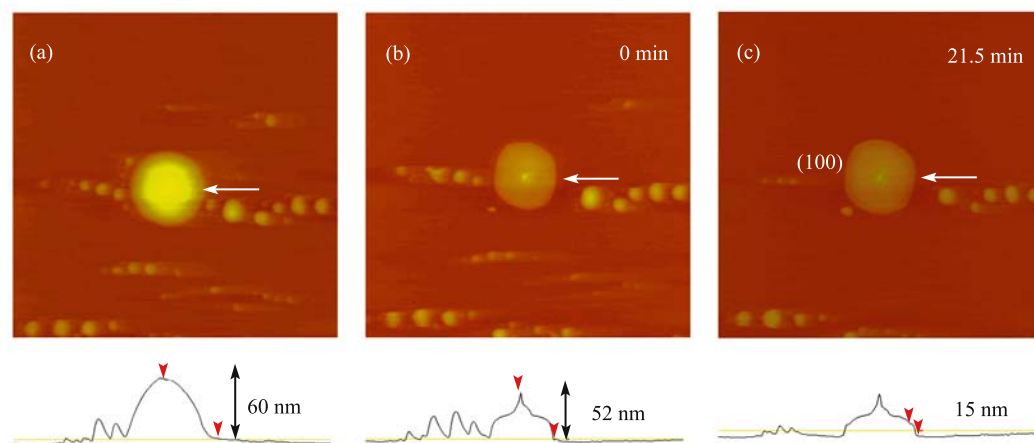**Fig. 3** *In-situ* AFM images of tip-induced crystallization of the PEO ($M_n = 1.0 \times 10^4$ g/mol) on the mica surface by nanoindentation
The AFM height images of (a) and (b, c) were obtained before and after indentation, respectively; the height profiles in the lower row of the figure are measured along the directions indicated by the white arrows in the AFM images; the size of the images is $10\,\mu m \times 10\,\mu m$

($M_n = 7.1 \times 10^3$ g/mol, 5.0×10^3 g/mol, and 3.0×10^3 g/mol), but no tip-induced crystallization was observed. We also found that even for the PEO fraction with $M_n = 1.0 \times 10^4$ g/mol the nanoindentation operation could not induce crystallization in every trial. Since the melt viscosity of the LMW PEO fraction is low, the molecules may easily detach from the AFM tip when the tip is pulled out of the droplet. Therefore, there is no sufficient perturbation for inducing nucleation. On the contrary, we found that the nanoindentation was effective when the relatively high molecular weight PEO sample ($M_n = 1.0 \times 10^5$ g/mol) was studied. At $T_c < 59°C$, the nanoindentation with a suitable tip force (trig threshold > 0.2 V) could readily cause the PEO crystallization. The results preliminarily demonstrate a molecular weight dependence of the tip-induced crystallization by nanoindentation, namely, the higher the molecular weight (thus the higher melt viscosity) of the PEO, the easier AFM-tip-induced crystallization will be.

In summary, we have investigated the effect of AFM tip on PEO melt crystallization on a mica surface. The lateral perturbation by the AFM tip in hard-tapping mode or in scratch mode cannot induce crystallization for the LMW PEO fractions ($M_n \leqslant 1.0 \times 10^4$ g/mol), while the longitudinal perturbation in nanoindentation mode can induce the formation of a nucleus, which will lead to the flat-on lamellar growth for the PEO with $M_n \geqslant 1.0 \times 10^4$ g/mol. However, for the PEO fractions with $M_n < 1.0 \times 10^4$ g/mol, the nanoindentation cannot induce crystallization. This indicates that the AFM-tip-induced crystallization of PEO is dependent on the molecular weight (viscosity).

References

1. Pearce R, Vancso G J. Imaging of melting and crystallization of poly(ethylene oxide) in real-time by hot-stage atomic force microscopy. Macromolecules, 1997, 30: 5843–5848

2. Pearce R, Vancso G J. Observations of crystallization and melting in poly(ethylene oxide)/poly(methyl methacrylate) blends by hot-stage atomic-force microscopy. J Polym Sci: Polym Phys, 1998, 36: 2643–2651

3. Vancso G J, Beekmans L G, Pearce R, Trifonova D, Varga J. From microns to nanometers: Morphology development in semicrystalline polymers by scanning force microscopy. J Macromol Sci Phys, 1999, B38: 491–503

4. Li L, Chan C M, Li J X, Ng K M, Yeung K L, Weng L T. A direct observation of the formation of nuclei and the development of lamellae in polymer spherulites. Macromolecules, 1999, 32: 8240–8242

5. Lei Y G, Chan C M, Li J X, Ng K M, Wang Y, Jiang Y, Li L. The birth of an embryo and development of the founding lamella of spherulites as observed by atomic force microscopy. Macromolecules, 2002, 35: 6751–6753

6. Godovsky Y K, Magonov S N. Atomic force microscopy visualization of morphology and nanostructure of an ultrathin layer of polyethylene during melting and crystallization. Langmuir, 2000, 16: 3549–3552

7. Magonov S N, Reneker D H. Characterization of polymer surfaces with atomic force microscopy. Annu Rev Mater Sci, 1997, 27: 175–222

8. Hare E F, Zisman W A. Autophobic liquids and the properties of their adsorbed films. J Phys Chem, 1955, 59: 335–340

9. Reiter G, Sommer J U. Crystallization of adsorbed polymer monolayers. Phys Rev Lett, 1998, 80: 3771–3774

10. Reiter G, Sommer J U. Polymer crystallization in quasi-two dimensions. I. Experimental results. J Chem Phys, 2000, 112: 4376–4383

11. Schnherr H, Frank C W. Ultrathin films of poly(ethylene oxides) on oxidized silicon. 1. Spectroscopic characterization of film structure and crystallization kinetics. Macromolecules, 2003, 36: 1188–1198

12. Zhai X M, Wang W, Zhang G L, He B L. Crystal pattern formation and transitions of PEO monolayers on solid substrates from nonequilibrium to near equilibrium. Macromolecules, 2006, 39: 324–329

13. Cheng Stephen Z D, Chen J H. Nonintegral and integral folding crystal growth in low-molecular mass poly(ethylene oxide) fractions. III. Linear crystal growth rates and crystal morphology. J Polym Sci: Polym Phys, 1991, 29: 311–327